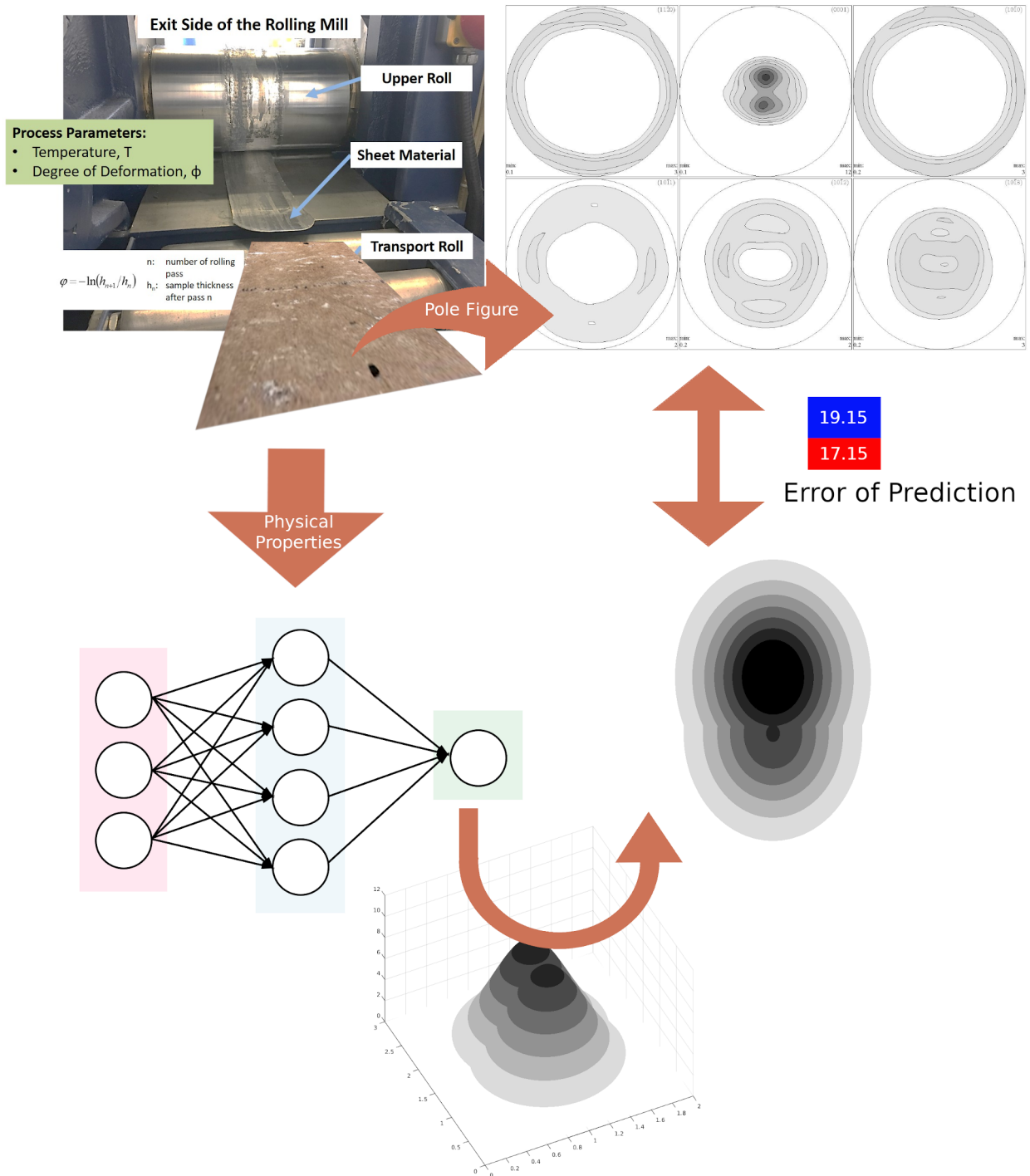# Graphical Abstract

Enabling intelligent Mg-sheet processing utilizing efficient machine-learning algorithm

Mohamadreza Shariati,Wolfgang E. Weber,Jan Bohlen,Gerrit Kurz,Dietmar Letzig,Daniel Höche

Highlights

Enabling intelligent Mg-sheet processing utilizing efficient machine-learning algorithm

Mohamadreza Shariati,Wolfgang E. Weber,Jan Bohlen,Gerrit Kurz,Dietmar Letzig,Daniel Höche

- Process-structure-property correlation for AZ31 based on machine learning is realized

- Machine learning algorithm to be applied for limited data sets is developed

- Approach for intelligent processing is suggested

Enabling intelligent Mg-sheet processing utilizing efficient machine-learning algorithm[⋆]

Mohamadreza Shariati[a,∗,1], Wolfgang E. Weber[a], Jan Bohlen[b], Gerrit Kurz[b], Dietmar Letzig[b] and Daniel Höche[b,∗∗]

[a]*Chair of Structural Analysis,* HELMUT-SCHMIDT-*University / University of the Federal Armed Forces Hamburg, D-22043 Hamburg, Germany*
[b]*MagIC - Magnesium Innovation Centre, Institute of Materials Research* HELMHOLTZ-*Zentrum Geesthacht, D-21502 Geesthacht, Germany*

ABSTRACT

Process - property relationship control during magnesium sheet manufacturing is demanding due to the complexity of involved interacting physics and the sensitivity of the system to small changes. Here, data science might help to extract crucial information on interdependencies between processing parameters and sheet quality. In this work we show that utilizing a dedicated machine learning algorithm enables the possibility to correlate materials properties and processing parameters without knowing the physics based on a relatively small training data set. For Mg-AZ31 alloy we show that e. g. crystallographic texture can be reliably predicted from mechanical measurement data sets. Combined with process parameters a manufacturing data space is generated. In the future with access to more data it is proposed that applying our approach might allow predicting and controlling in-situ the twin-roll casting process route.

1. Introduction

Currently, magnesium based materials are used for lightweight components in vehicles, for biomedical applications or are handled as candidate to become anode material for post-Li energy storage devices. Most common in the automotive sector is the processing as die castings. Die casting allows the fabrication of components with a complex geometry. Nevertheless, the mechanical properties of the die cast components often do not meet essential requirements with regard to endurance, strength, ductility, etc. A promising alternative for thin, large area parts, such as automotive body components, are components made from magnesium sheets. Relevant deep drawn parts are characterized by high quality surfaces without pores and superior mechanical properties in comparison to die cast components. However, this requires production of high-performance dies, as shown by a promising approach by e. g. CURBACH et al. [12]. To bring magnesium sheet components or even Mg-foils for future energy applications to the market, it will be necessary to fabricate material with competitive properties in an economic production process. A favored processing route for the production of magnesium sheets is a two step process. The first step is the production of thin strips by twin-roll casting [3]. In the second step these strips will be rolled to final gauge in a conventional rolling process. Twin-roll casting of thin strips combines solidification and rolling into one single production step. Thus, it saves a high number of rolling and annealing passes in comparison to the conventional rolling process from the slab [20, 18, 11, 22, 1]. In the twin-roll casting

process liquid metal is cast over a pipe into a tundish. The melt is then dragged into the roll gap of a pair of counter rotating, internally cooled rolls. The metal solidifies upon contact with the cooled rolls and is rolled to a strip. These strips are then used as feedstock material having a significant impact on final sheet properties and property changes during the subsequent rolling process. This conventional rolling process represents the established production method for the manufacturing of sheets. The used feedstock material is passed through a pair of rolls, whereby the roll gap remains smaller than the thickness of the feedstock, such that plastic deformation occurs. The sheet properties, e.g. the mechanical properties, can be related to the applied rolling process parameters, a sequence of individual hot rolling passes followed by a heating phase [5]. The rolling temperature is an essential process parameter, which e. g. activates important deformation mechanisms in Mg alloys. A coarser grained microstructure was obtained at higher rolling temperatures as a result of dynamic recrystallization and grain growth. Furthermore, the texture sharpness decreases with increasing rolling temperature [6, 17, 10]. The degree of deformation (i. e. the amount of plastic strain in the thickness direction) per rolling step also influences the microstructure and texture, as it determines the strain rate and the extent of deformation before recovery and recrystallization of the deformed microstructure during intermediate annealing [9]. This paper reports on results of rolling experiments on such twin-roll cast strips of magnesium alloy AZ31 (Mg-3Al-1Zn-Mn) with different rolling parameters like degree of deformation ϕ and temperature T and its interdependencies. Herein, the degree of deformation ϕ is equal to the plastic strain in the thickness-direction of the metal sheet due to the twin-roll casting.

It will be shown that besides the very complex interacting physics the prescriptive application of data science enables process control within a manufacturing data space. In

the future the data space might be applied to control actors within an intelligent sheet manufacturing route.
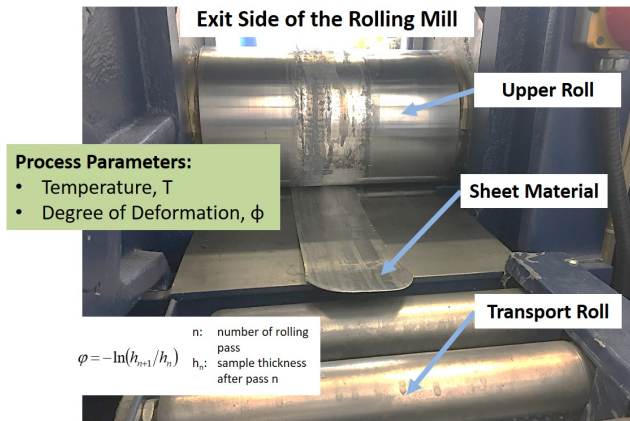

Figure 1: Varied process parameters, rolling temperature T and degree of deformation ϕ

2. Experimental testing and (training) data generation

2.1. Rolling of magnesium sheets

For the rolling trials, twin-roll cast feedstock material of the commercial magnesium alloy AZ31 was used. The strips had a width of 350 mm and are twin-roll cast at a temperature T of 650 °C and with a casting speed of 1.8 m/min, [14]. The AZ31 strip was used in the as-twin-roll cast condition and rolled at three different rolling temperatures, 350 °C, 400 °C, and 450 °C, as well as three different degrees of deformation per pass, $\phi = 0.1$, $\phi = 0.2$, and $\phi = 0.3$, [15]. Prior to the rolling procedure the strips were heated for 30 min to the respective rolling temperature. Between the following rolling passes, the rolled samples were again reheated to the rolling temperature for 15 min. After the final rolling pass the sheets were air cooled. The rolling speed was 10 m/min and a water-soluble oil based lubricant was used.

2.2. Micrographs and texture measurements

After rolling, the microstructures of the materials were analyzed using optical microscopy. Standard metallographic sample preparation techniques were employed and an etchant based on picric acid was used to reveal grains and grain boundaries, [13]. Texture measurements in the sheets were performed on the sheet mid-planes using a Panalytical X-ray diffractometer setup and CuK_{α} radiation. Six pole figures were measured up to a tilt of 70° which allows recalculation of full pole figures using the open source software routine MTEX, see e. g. [2]. The (0001) pole figure is used in this work to present the texture of the sheets at the midplane.

2.3. Mechanical testing

In order to see how the different process parameters do influence the mechanical properties of the sheets, stress-strain curves were measured by tensile tests according to DIN EN 10002. Testing was performed on samples extracted from the sheet in rolling direction, 45° to rolling direction and in the transverse orientation. For statistical verification, 4 tensile tests were performed per test parameter. Curves were analyzed according to mechanical standards for tensile yield strength (TYS), ultimate tensile strength (UTS) and elongation of fracture (A).

3. Data and data analysis

3.1. Experimental data

Figure 2 displays the microstructures from longitudinal sections of the as-rolled sheets of alloy AZ31. The microstructures of all sheets are not fully recrystallized. With increasing rolling temperature the amount and size of the not recrystallized grains decreases, see e. g. [15]. The sheets rolled at 450 °C with the degree of deformation of $\phi = 0.1$ are nearly fully recrystallized, [15]. With increasing degree of deformation the amount and size of the deformed grains are increasing again. In the sheets rolled at 350 °C and a degree of deformation of $\phi = 0.3$ shear bands are observed [15]. Obviously, only two process control variables need to be implemented and become part of the manufacturing data space:

- Data for the data space: T, ϕ

The (0001) pole figures (basis plane defined via x and y coordinates) of nearly all the sheets show detectable pronounced split peaks towards the rolling direction and an angular distribution to the transverse direction, cf. [15]. This texture can be associated to the high amount of unrecrystallized grains in the rolled material [21]. Because of this effect the (0001) pole figure of the sheet rolled at 450 °C and a degree of deformation of $\phi = 0.1$ show a single peak, see [15]. The tendency to develop such a texture increases with increasing rolling temperature and decreasing degree of deformation per pass and is consistent with further recrystallized microstructures, see e. g. [15]. For the manufacturing data space we reduce the amount of data describing the intensity $I_{0001}(x, y)$ of the pole figure by only using the two (or via convolution – single) maxima values and by assuming single peak GAUSSian like profiles. Since there is no physical meaning of the position of the higher peak maximum (depends on the sample placement direction within XRD machine) it is allowed to define an additional constraint to lower the final error:

- Data for the data space: $I_{0001-1,2}$ maximum or in short form p_1, p_2 with $p_1 \geq p_2$ by definition
  (Remark: This approximation in general is not a valid texture description, however mathematical applicable for our use case.)

Figure 3 displays the stress-strain curves of the specimen taken in the rolling direction, representative for all tensile tests. The stress-strain curves in Figure 3 respectively the data in Table 1 show in tendency that the elongation at fracture increases with increasing temperature, whereas the
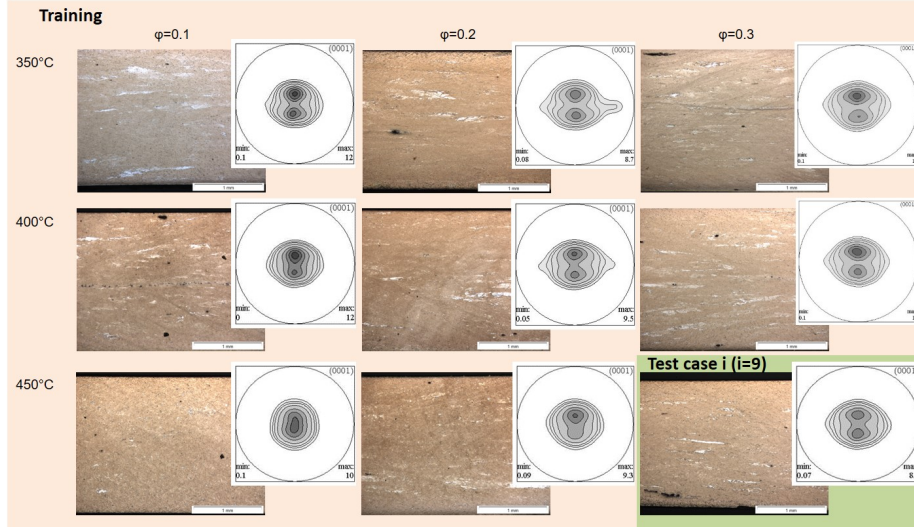
Figure 2: Cross-section micrograph and respective pole figures of (0001), taken from [15]. Usage of data in Section 3 is indicated

yield strength and ultimate tensile strength decreases. This tendency also corresponds to the stress-strain curves taken in transverse direction and 45° to the rolling direction, see e. g. [15]. This inverse behavior can be observed at increasing degree of deformation. This material behavior is understood by a higher work hardening of the material at higher deformation degrees. At higher rolling temperatures recrystallization effects weaken the material hardening and lead to increased formability of the sheet material, i. e. the fracture strain in the context of this work, [15]. Consequently, the entire mechanical property design space will be described by only three numbers per three cases determined by standard tensile testing according to DIN EN 10002.

- Data for the data space: TYS, UTS, and A in three directions (longitudinal, transverse, 45°) to rolling (given in Table 1)

In a data space of dimension 10 ($T, \phi, I_{0001-1,2}$, TYS, UTS, A, three directions) with only 9 data sets (8 for training and 1 for testing) an as best as possible process-structure
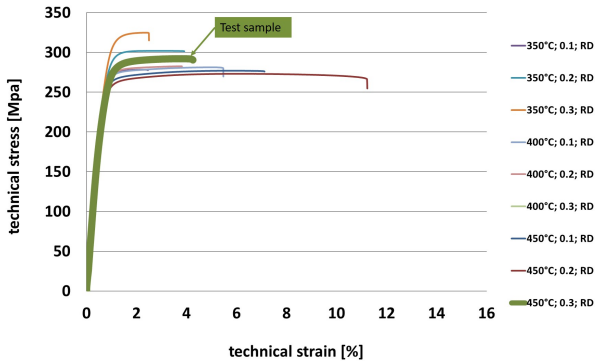

Figure 3: Stress strain curves in rolling direction (RD), taken from [15]

property correlation with minimized error is targeted. Therefore, a dedicated machine learning (ML) algorithm is implemented.

3.2. Feedforward Neural Network

In this context we are using the most basic type of neural networks, namely, multi layer perceptron or multilayer feedforward network. Besides the simple structure it has the capability of replicating nonlinear maps by adding hidden layers and increasing the number of nodes at each layer. The word "hidden" here refers to the fact that these layers are located between input and output layers, [8]. For a neuron i, let $\{a_1, \ldots, a_m\}$ be outputs of neurons $1, \ldots, m$ in the previous layer, which are connected to neuron i with weights $\{w_{1i}, \ldots, w_{mi}\}$. The adder for summing the input signals to neuron i is defined as

$$\Sigma_i = \sum_{j=1}^{m} w_{ji} a_j + b_i \quad , \tag{1}$$

where $b_i \in \mathbb{R}$ is a bias. The output of neuron i is computed by $f(\Sigma_i)$. The activation function $f(\cdot)$, considered to be a log-sigmoid function of the form

$$f(\Sigma_i) = \frac{1}{1 + \exp(-\Sigma_i)} \quad . \tag{2}$$

Note that both in the input and output layer, the neurons have identical activation functions. Assigning the input units, the output of the network can be calculated as a vector-valued function of N unknown connection weights $F(w_1, \ldots, w_N; \vec{x})$ for an input vector $\vec{x}$. Note the dimension of function $F(\vec{w}; \vec{x})$ is equal to the number of outputs. In order to compute the network connection weights, we used the BAYESian regularization method which is discussed in [4]. The error function against the expected output y of the training set for BAYESian

Table 1
Collection of sheet property data (TYS and UTS in [MPa])

degree of deformation data points (D_i)		$\phi = 0.1$			$\phi = 0.2$			$\phi = 0.3$		
		D_1	D_2	D_3	D_4	D_5	D_6	D_7	D_8	D_9
45°	TYS	219	227	231	243	222	216	239	222	237
	UTS	266	271	270	292	271	267	303	281	283
	A	6.27	7.22	6.56	5.62	7.24	11.54	5.37	8.14	8.83
transverse	TYS	214	227	226	236	220	217	234	221	223
	UTS	267	270	272	294	273	275	302	284	273
	A	2.59	1.93	2.57	1.55	1.79	4.85	2.34	3.27	2.95
longitudinal	TYS	261	260	252	274	252	240	284	258	250
	UTS	279	281	277	305	280	273	323	292	290
	A	1.76	4.86	6.72	3.38	3.46	10.57	1.91	2.77	4.99
temperature °C		350	400	450	350	400	450	350	400	450

regularization is of the form

$$E(w) = \frac{\beta}{2} \sum_{n=1}^{S} (F(w; x) - y)^2 + \frac{\alpha}{2} \|w\|^2 \quad , \qquad (3)$$

where S is the number of all training data points and α, β are hyperparameters for weights prior probabilities and variance of GAUSSian distribution that is considered for a weight. The reasons for choosing BAYESian regularization are, first, the method requires no validation step which means the available data only is used for training and testing of the network. Second, it gives the most probable possibility for connection weights. The latter is important as here we want to observe if there exist a mapping from physical properties to the coefficients of an assumed basis for pole figures. The error function (3) is to be minimized, here, by using the well-known LEVENBERG-MARQUART algorithm that is endowed with GAUSS-NEWTON approximation to the HESSian matrix as introduced in [7]. The method finds a local minimum, which however may not be the global solution.

For the pole figures we assume a convolution of two GAUSSian functions with a maximum value similar to the pole value.

$$\kappa(x, y) = \sum_{i=1}^{2} p_i \exp(-\frac{(x - x_i)^2}{2c_1^2} - \frac{(y - y_i)^2}{2c_2^2}) \quad , \quad (4)$$

where (x_i, y_i) is the CARTESian coordinates (x, y basis plane) of the poles and p_i is the value of the pole maximum intensity. c_1 and c_2 are constants here, however they can be also dependent on the poles ($c_{1,i}$ and $c_{2,i}$).

3.3. Data analysis

The dimension of data is 10. Since we use a relatively small set of data, at first, a dimensionality reduction is applied on the data.

To do this, the so called Local Linear Embedding (LLE) technique, first introduced in [19], is chosen by a neighborhood graph of size K. This technique is classified as a local nonlinear technique, which is promising compared to the traditional linear methods such as Principal Component and

Linear Discriminant Analysis, cf. [16]. One advantage of this technique is that in order to keep the distance of data points, it preserves the manifold through neighborhood graphs. Preserving the manifold is of high importance in our study, since we look for the mapping from meaningful input parameters that in fact have a natural dependency. If the manifold changes, it means the natural dependency is changed. Another advantage is that, as a local technique, it allows for successful embedding of non-convex manifolds. Trivially the latter is critical for our study, as we have no prior information over the manifold. The aimed dimension for dimensionality reduction is set to 4. The result of Maximum Likelihood Estimator with and without temperature factor was 2.6. Therefore a choice of 4 seems to be an appropriate choice. To have a unique solution for dimensionality reduction as in Roweis et al. [19] the logical choice is $K > 4$, which leads to a system with more equations than unknowns. We set $K = 5$ in our observations. To create more data points artificially, we set one data point aside for testing. Then the remaining data is regenerated 4 times with a maximum error bound of 1% that comes from a GAUSSian distribution. In this way we have 40 data entries for training and 1 data for testing.

A feedforward network with one hidden layer of size 4 is applied. The bias only exists on hidden layer and it is defined as a constant vector in $\mathbb{R}^4$. The total number of unknowns thus is $4 \times 4 + (4 + 1) \times 2 = 26$, and equals the number of connections between input and hidden layer and connections between hidden layer including bias and output layer. The input and output data is normalized to $[-1, 1]$ automatically by the $feedforwardnet()$ function in MATLAB. The GAUSSian function as given with Eq. (4) considered with $2c_1^2 = 0.25$, $2c_2^2 = 0.5$, $(x_1, y_1) = (1, 1.75)$, and $(x_2, y_2) = (1, 1.25)$, p_1, p_2 are the network output data. With this setting shown in Fig. 4, we step forward to computation.

3.4. Implementation and Error analysis

MATLAB Deep Learning Toolbox^{TM} (formerly Neural Network Toolbox^{TM}) $R2019a$ is used for the implementation. It minimizes the error as given with Eq. (3) by an algorithm as documented in [7] and then seeks for the best combination of weights, which results in a network that generalizes well. The search for the best weight combination, after
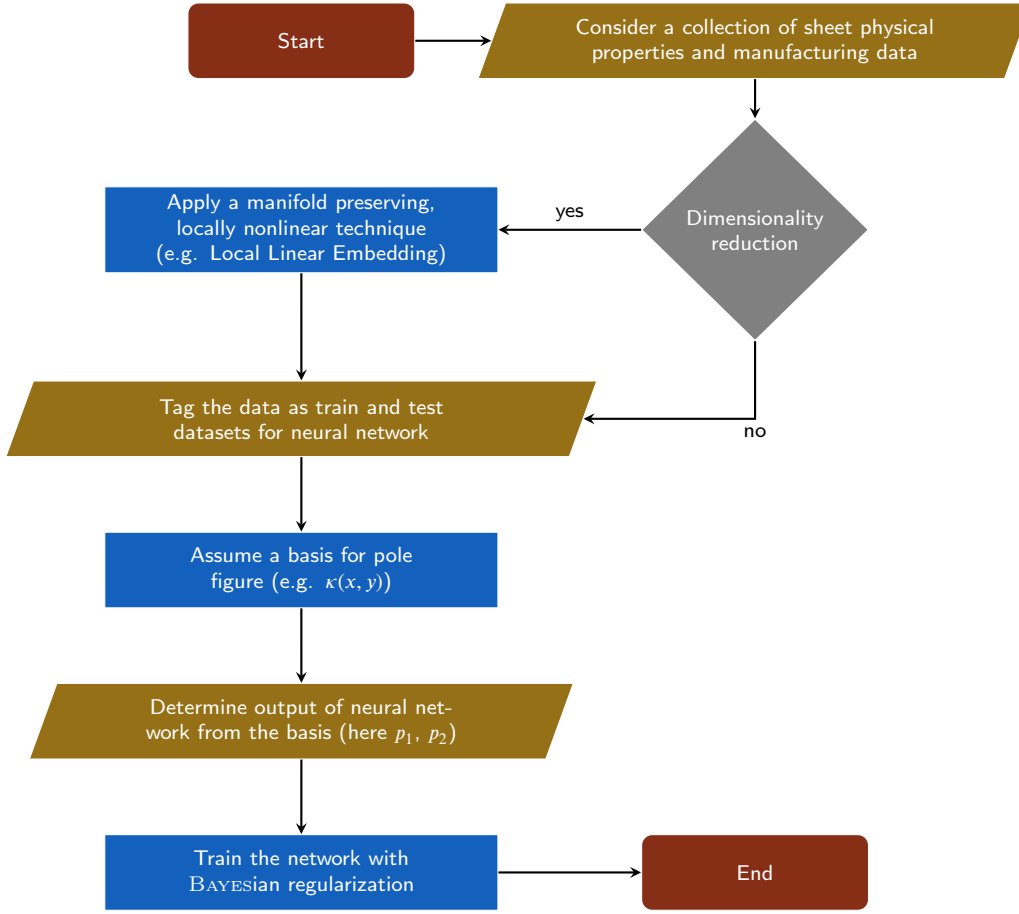
Figure 4: Proposed Machine Learning Algorithm

the minimization solution has been reached, is the source of high dependency on the random seed. We observed that the error for the testing data point varies between different random seeds. In order to have a meaningful error analysis we consider

- A network is trained 500 times starting from a fixed random seed by using MATLAB function $rng(4e5)$. The error vector of the test is defined as

$$\begin{bmatrix} e_1 \\ e_2 \end{bmatrix} = \begin{bmatrix} e_1^j \\ e_2^j \end{bmatrix} \quad j := \min_i \max\{e_1^i, e_2^i\}, \quad i = 1, \dots, 500 \quad .$$

  where at each experiment $i = 1, \dots, 500$, $e_1^i = |p_1 - p_1^i|$ and similarly $e_2^i = |p_2 - p_2^i|$.

- The relative error vector here is defined as

$$\begin{bmatrix} e_1^r \\ e_2^r \end{bmatrix} = \begin{bmatrix} e_1/I_1 \\ e_2/I_2 \end{bmatrix}$$

  where

$$I_1 := \max_{D_i} p_1 - \min_{D_i} p_1$$

  and similarly

$$I_2 := \max_{D_i} p_2 - \min_{D_i} p_2$$

  .

- We use every data point, once as the test and train the network with remaining 8 data points. It gives us a more comprehensive evaluation considering the data availability limitations.

The numerical result for experimental pole figure data points (p_1, p_2) from Figure 2 are as shown in Table 2. The experimental and predicted pole figures can be seen in Figure 5. The error bars in Figure 5 shows the defined relative error for each data point. As it can be read from the Figure 5, the relative error is at its peak in D_1 and D_9. Interestingly at these points the minimum and maximum of temperature T and degree of deformation ϕ is attained, which are the two independent parameters in this experiment. From physical point of view, for the points D_1 and D_9 no information (data point) is available on respectively, lower and higher ϕ and T values. Naturally, the map at these points is not well presented and consequently, the network was not able to achieve better prediction at them. Nevertheless, the average relative error of all predictions is $\begin{bmatrix} 19.15\% \\ 17.15\% \end{bmatrix}$. Considering the limits on the amount of available data this is a convenient error bound.

Table 2
Error of prediction for each data point as test

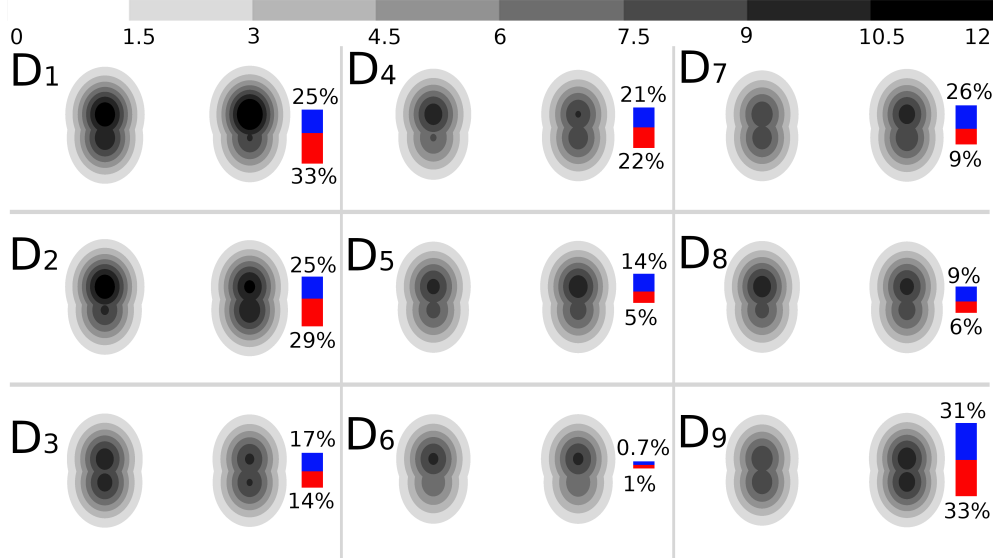|	D_1	D_2	D_3	D_4	D_5	D_6	D_7	D_8	D_9
p_1	12	12	10	10	9.5	9.3	8.7	10	8.7
p_1^j	13.08	10.91	9.25	9.09	10.12	9.33	9.83	9.6	10.05
e_1	1.08	1.09	0.75	0.91	0.62	0.03	1.13	0.4	1.35
p_2	10.3	9.2	9.7	7.6	8.0	7.2	8.5	8.0	8.6
p_2^j	9.09	10.41	9.1	8.51	8.2	7.25	8.85	8.24	9.83
e_2	1.21	1.21	0.6	0.91	0.2	0.05	0.35	0.24	1.23

Figure 5: For each data point D_i experimental result at the left (targeted pole figure) vs. the algorithm based prediction at the right. The relative error is represented as red bar for the pole intensity p_1 and blue for p_2. Note that each column has fixed ϕ and each row fixed T.

3.5. Manufacturing data space and testing

After the data space is defined and the system trained the approach is tested for the cases shown in Figures 2, 3 and results in pole figure data as illustrated in Figure 5. The aim is to verify the algorithm for application within a manufacturing route. While the two GAUSSian peaks of $I_{0001}(p_1, p_2)$ were determined via experiment as shown in Table 2. Obviously, based on this very limited data set, the algorithm is capable to correctly predict pole figure data in most cases. To manage deviations at the boundary of the parameter window and to reduce errors additional training data is required. Nevertheless, the algorithm predicts on average with an accuracy less than 20%. With respect to the very limited data space the process-structure-property correlation is acceptable.

Figure 6 illustrates how the application of the algorithm simplifies the data space with D_9 as a representative test sample. The algorithm predicts $\begin{bmatrix} 10.1 \\ 9.8 \end{bmatrix}$ which is still in good agreement to the experimental values $\begin{bmatrix} 8.7 \\ 8.6 \end{bmatrix}$ despite the fact that the test data is allocated at the parameter window boundary. Consequently, tolerating a certain error bound, a very limited manufacturing data space enables end-users to ef-

ficiently and fast adapt process parameters. Applying our algorithm in a prescriptive manner within a software and actor control unit, in-situ or better intelligent processing is enabled. The capabilities of the algorithm and the efficiency in prediction and correlation might be extended by adding more data form literature, image analysis, monitoring data or materials / process simulations as indicated in Figure 6.

4. Conclusions

The results reveal that the rolling process has got a significant influence on the resulting sheet properties. It could be shown that higher rolling deformation degrees and lower process temperature lead to higher strength but lower formability in the sheet material. In contrast, higher rolling temperatures improve the formability but weaken the strength of the sheets. Obviously, knowledge- and physics based process – property correlation is demanding. As a consequence, an efficient ML based approach is suggested to overcome this issue. It should be indicated that for a further reduction of the error bounds, cost-effectiveness has to be taken into account, cf. [23].

The developed algorithm applies dimensionality reduction, a feedforward neural network, BAYESian regularization including precise error minimization and analysis, and allows
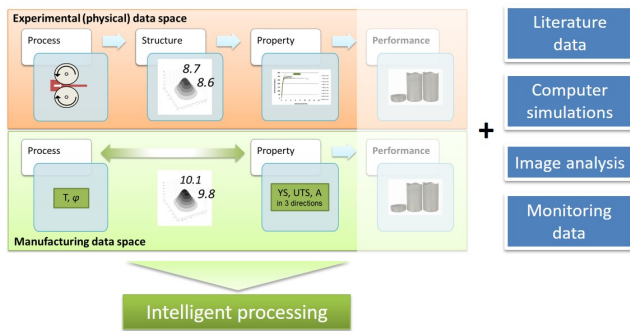
Figure 6: Condensing the huge experimental data space for wrought processing to a limited manufacturing data space enabling fast intelligent process adaption (here for example D_9). Data space extension by literature data, physics based simulations, image and other monitoring data to guarantee reproducible processing is recommended.

to look for correlation within very limited data spaces. Finally, based on a limited data set of process parameters, mechanical properties and pole figure data, the entire routine was tested. Application on a test scenario in order to predict pole figures (data) simply from stress-strain curve measurements and two processing parameters shows excellent correlation with respect to the data space dimension. If we take a look into the future the approach might be used to create efficient manufacturing data spaces enabling intelligent processing routes and Industry 5.0.

Acknowledgment

Data availability

The raw data required to reproduce these findings are available to download from [https://github.com/mrshariati/Mg-sheet-machine-learning-algorithm]. The processed data required to reproduce these findings are available to download from [https://github.com/mrshariati/Mg-sheet-machine-learning-algorithm].

CRediT authorship contribution statement

Mohamadreza Shariati: ML Methodology, Software, Writing. **Wolfgang E. Weber:** Data interpretation, Writing. **Jan Bohlen:** Data interpretation, Writing. **Gerrit Kurz:** Experimental data, Data evaluation, Writing. **Dietmar Letzig:** Conceptualization of this study. **Daniel Höche:** Conceptualization of this study, Data curation, Writing - Original draft preparation.

References

[1] Aljarrah, M., Essadiqi, E., Kang, D., Jung, I.H., 2011. Solidification microstructure and mechanical properties of hot rolled and annealed mg sheet produced through twin roll casting route. Materials Science Forum 690, 331–334. doi:10.4028/www.scientific.net/MSF.690.331.

[2] Bachmann, F., Hielscher, R., Schaeben, H., 2010. Texture analysis with mtex - free and open source software toolbox. Solid State Phenomena 160, 63–68.

[3] Basson, F., Letzig, D., 2010. Aluminium twin roll casting transfers benefits to magnesium. Aluminium International Today , 19–21.

[4] Bishop, C.M., 1995. Bayesian Methods for Neural Networks. Technical report ed., Aston University, Birmingham.

[5] Bohlen, J., Kurz, G., Yi, S., Letzig, D., 2012. Rolling of magnesium alloys, in: Advances in Wrought Magnesium Alloys. Elsevier, pp. 346–375.

[6] Chino, Y., Mabuchi, M., 2009. Enhanced stretch formability of mg–al–zn alloy sheets rolled at high temperature (723 k). Scripta Materialia 60, 447–450.

[7] Foresee, F.D., Hagan, M.T., 1997. Gauss-newton approximation to bayesian learning. Proceedings of International Conference on Neural Networks (ICNN'97) 3, 1930–1935. doi:10.1109/ICNN.1997.614194.

[8] Haykin, S.S., 2009. Neural Networks and Learning Machines. 3th ed., Pearson.

[9] Jeong, H.T., Ha, T.K., 2007. Texture development in a warm rolled az31 magnesium alloy. Journal of Materials Processing Technology 187, 559–561.

[10] Jin, L., Dong, J., Wang, R., Peng, L., 2010. Effects of hot rolling processing on microstructures and mechanical properties of mg–3% al–1% zn alloy sheet. Materials Science and Engineering: A 527, 1970–1974.

[11] Kawalla, R., Oswald, M., Schmidt, C., Ullmann, M., Vogt, H.P., Cuong, N.D., 2008. Development of a strip-rolling technology for mg alloys based on the twin-roll-casting process. TMS Magnesium Technology , 177–182.

[12] Kleiner, M., Curbach, M., Tekkaya, A.E., Ritter, R., Speck, K., Trompeter, M., 2008. Development of ultra high performance concrete dies for sheet metal hydroforming. Production Engineering 2, 201–208. doi:10.1007/s11740-008-0099-z.

[13] Kree, V., Bohlen, J., Letzig, D., Kainer, K., 2004. The metallographical examination of magnesium alloys. Practical Metallography 5, 233–246.

[14] Kurz, G., Bohlen, J., Letzig, D., Kainer, K., 2013. Influence of process parameters on twin roll cast strip of the alloy az31. Materials Science Forum 765, 205–209. doi:10.4028/www.scientific.net/MSF.765.205.

[15] Kurz, G., Pakulat, S., Bohlen, J., Letzig, D., 2015. Rolling twin roll cast magnesium strips with varied temperature and degree of deformation. Materials Today. Proceedings 2S, 39–44.

[16] van der Maaten, L.J.P., 2007. An Introduction to Dimensionality Reduction Using Matlab - Bayesian Methods for Neural Networks. Report MICC 07-07 ed., MICC, Maastricht University.

[17] Nestler, K., Bohlen, J., Letzig, D., Kainer, K.U., 2007. Influence of process parameters on the mechanical properties of rolled mangnesium zm21-sheets. Magnesium Technology 2007 , 95–100.

[18] Park, S.S., Bae, G.T., Lee, J.G., Kang, D.H., Shin, K.S., Kim, N.J., 2007. Microstructure and mechanical properties of twin-roll strip cast mg alloys. Materials Science Forum 539/543, 119–126.

[19] Roweis, S.T., Saul, L.K., 2000. Nonlinear dimensionality reduction by locally linear embedding. Science 290, 2323–2326. doi:10.1126/science.290.5500.2323.

[20] St John, D.H., 2007. Overview of current international magnesium research and recent cast crc developments. Advanced Materials Research 29-30, 3–8.

[21] Victoria-Hernandez, J., Yi, S., Bohlen, J., Kurz, G., Letzig, D., 2014. The influence of the recrystallization mechanisms and grain growth on the texture of a hot rolled az31 sheet during subsequent isochronal annealing. Journal of Alloys and Compounds 616, 189–197.

[22] Watari, H., Haga, T., Paisarn, R., Koga, N., Davey, K., 2007. Mechanical properties and metallurgical qualities of sheets manufactured by

twin-roll casting. Key Engineering Materials 345/346, 165–168.

[23] Weber, W.E., Reuter, U., 2017. Fuzzy modeling of wave-shielding under consideration of cost-effectiveness for an efficient reduction of uncertainty. Advances in Engineering Software 109, 53–61. doi:10. 1016/j.advengsoft.2017.03.005.